A Facile Synthesis and Photoluminescent Properties of Redispersible CeF_3, CeF_3:Tb^{3+}, and CeF_3:Tb^{3+}/LaF_3 (Core/Shell) Nanoparticles

Z. L. Wang,[†] Z. W. Quan,[†] P. Y. Jia,[†] C. K. Lin,[†] Y. Luo,[†] Y. Chen,[‡] J. Fang,[‡] W. Zhou,[‡] C. J. O'Connor,[‡] and J. Lin*,[†]

Key Laboratory of Rare Earth Chemistry and Physics, Changchun Institute of Applied Chemistry, Chinese Academy of Sciences, Changchun 130022, Graduate School of the Chinese Academy of Sciences, Beijing 100049, P. R. China, and Advanced Materials Reseach Institute, College of Science, University of New Orleans, New Orleans, Louisiana 70148

Received October 27, 2005. Revised Manuscript Received February 14, 2006

CeF_3, CeF_3:Tb^{3+}, and CeF_3:Tb^{3+}/LaF_3 (core/shell) nanoparticles were prepared by the polyol method and characterized by X-ray diffraction (XRD), transmission electron microscopy (TEM), X-ray photoelectron spectra (XPS), UV−vis absorption spectra, photoluminescence (PL) spectra, and lifetimes. The results of XRD indicate that the obtained CeF_3, CeF_3:Tb^{3+}, and CeF_3:Tb^{3+}/LaF_3 (core/shell) nanoparticles crystallized well at 200 °C in diethylene glycol (DEG) with a hexagonal structure. The TEM images illustrate that the CeF_3 and CeF_3:Tb^{3+} nanoparticles are spherical with a mean diameter of 7 nm. The growth of the LaF_3 shell around the CeF_3:Tb^{3+} core nanoparticles resulted in an increase of the average size (11 nm) of the nanopaticles as well as in a broadening of their size distribution. These nanocrystals can be well-dispersed in ethanol to form clear colloidal solutions. The colloidal solutions of CeF_3 and CeF_3:Tb^{3+} show the characteristic emission of Ce^{3+} 5d−4f (320 nm) and Tb^{3+} $^5D_4$−^7F_J (J = 6−3, with $^5D_4$−$^7F_5$ green emission at 542 nm as the strongest one) transitions, respectively. The emission intensity and lifetime of the CeF_3:Tb^{3+}/LaF_3 (core/shell) nanoparticles increased with respect to those of CeF_3:Tb^{3+} core particles. This indicates that a significant amount of nonradiative centers existing on the surface of CeF_3:Tb^{3+} nanoparticles can be eliminated by the shielding effect of LaF_3 shells. Finally, the energy transfer from Ce^{3+} to Tb^{3+} was investigated in CeF_3:Tb^{3+} nanoparticles in detail.

I. Introduction

Inorganic luminescent materials with nanosale dimensions have found many potential applications, such as light-emitting devices, low-threshold lasers, optical amplifiers, biological fluorescence labeling, and so forth.[1] However, due to nonradiative decay from defects on the surface of the nanocrystals, the luminescence efficiency of nanostructural materials is usually lower than that of the corresponding bulk materials.[2] To reduce these defects, the growth of a crystalline shell of a suitable inorganic material around each nanocrystal to form the core/shell structures has been regarded as an effective strategy to improve luminescent efficiency. This strategy has been successfully applied in II−VI and III−V semiconductor core/shell systems, such as CdSe/ZnS,[3] CdSe/CdS,[4] CdSe/ZnSe,[5] CdS/ZnS,[6] InP/ZnS,[7] InAs/InP, and InAs/CdSe[8] core/shell nanocrystals. In recent years, the synthesis of core−shell structural luminescent materials with luminescent lanthanide nanocrystals as cores and inert host compounds as shells has been reported by several groups.[1a,2a,9] These systems doped with lanthanide ions are based on two

* Corresponding author. E-mail address: jlin@ns.ciac.jl.cn.
[†] Chinese Academy of Sciences.
[‡] University of New Orleans.

(1) (a) Kömpe, K.; Borchert, H.; Storz, J.; Lobo, A.; Adam, S.; Möller, T.; Haase, M. *Angew. Chem., Int. Ed.* **2003**, *42*, 5513−5516. (b) Stouwdam, J. W.; Hebbink, G. A.; Huskens, J.; van Veggel, F. C. J. M. *Chem. Mater.* **2003**, *15*, 4604−4616. (c) Heer, S.; Lehmann, O.; Haase, M.; Güdel, H. *Angew. Chem., Int. Ed.* **2003**, *42*, 3179−3182. (d) Meiser, F.; Cortez, C.; Caruso, F. *Angew. Chem., Int. Ed.* **2004**, *43*, 5954−5957.
(2) (a) Bu, W.; Hua, Z.; Chen, H.; Shi, J. *J. Phys. Chem. B* **2005**, *109*, 14461−14464. (b) Li, Q.; Gao, L.; Yan, D. *Chem. Mater.* **1999**, *11*, 533−535.
(3) (a) Hines, M. A.; Guyot-Sionnest, P. *J. Phys. Chem.* **1996**, *100*, 468−471. (b) Talapin, D. V.; Rogach, A. L.; Kornowski, A.; Haase, M.; Weller, H. *Nano Lett.* **2001**, *1*, 207−211. (c) Dabbousi, B. O.; Rodriguez-Viejo, J.; Mikulec, F. V.; Heine, J. R.; Mattoussi, H.; Ober, R.; Jensen, K. F.; Bawendi, M. G. *J. Phys. Chem. B* **1997**, *101*, 9463−9475.
(4) (a) Peng, X.; Schlamp, M. C.; Kadavanich, A. V.; Alivisatos, A. P. *J. Am. Chem. Soc.* **1997**, *119*, 7019−7029. (b) Li, J. J.; Wang, Y. A.; Guo, W.; Keay, J. C.; Mishima, T. D.; Johnson, M. B.; Peng, X. *J. Am. Chem. Soc.* **2003**, *125*, 12567−12575. (c) Pan, D.; Wang, Q.; Jiang, S.; Ji, X.; An, L. *Adv. Mater.* **2005**, *17*, 176−179.
(5) (a) Danek, M.; Jensen, K. F.; Murray, C. B.; Bawendi, M. G. *Chem. Mater.* **1996**, *8*, 173−180. (b) Reiss, P.; Bleuse, J.; Pron, A. *Nano Lett.* **2002**, *2*, 781−784.
(6) (a) Manna, L.; Scher, E. C.; Li, L. S.; Alivisatos, A. P. *J. Am. Chem. Soc.* **2002**, *124*, 7136−7154. (b) Steckel, J. S.; Zimmer, J. P.; Coe-Sullivan, S.; Stott, N. E.; Bulović, V.; Bawendi, M. G. *Angew. Chem., Int. Ed.* **2004**, *43*, 2154−2158.
(7) Borchert, H.; Haubold, S.; Haase, M.; Weller, H.; McGinley, C.; Riedler, M.; Möller, T. *Nano Lett.* **2002**, *2*, 151−154.
(8) (a) Cao, Y. W.; Banin, U. *Angew. Chem., Int. Ed.* **1999**, *38*, 3692−3694. (b) Cao, Y. W.; Banin, U. *J. Am. Chem. Soc.* **2000**, *122*, 9692−9702.
(9) (a) Lehmann, O.; Kömpe, K.; Haase, M. *J. Am. Chem. Soc.* **2004**, *126*, 14935−14942. (b) Stouwdam, J. W.; van Veggel, F. C. J. M. *Langmuir* **2004**, *20*, 11763−11771. (c) Sudarsan, V.; van Veggel, F. C. J. M.; Herring, R. A.; Raudsepp, M. *J. Mater. Chem.* **2005**, *15*, 1332−1342. (d) Sivakumar, S.; van Veggel, F. C. J. M.; Raudsepp, M. *J. Am. Chem. Soc.* **2005**, *127*, 12464−12465. (e) Sudarsan, V.; Sivakumar, S.; van Veggel, F. C. J. M.; Raudsepp, M. *Chem. Mater.* **2005**, *17*, 4736−4742. (f) Buissette, V.; Giaume, D.; Gacoin, T.; Boilot, J.-P. *J. Mater. Chem.* **2006**, *16*, 529−539. (g) Buissette, V.; Moreau, M.; Gacoin, T.; Boilot, J.-P. *Adv. Funct. Mater.* **2006**, *16*, 351−355.

10.1021/cm052360x CCC: $33.50
Published on Web 03/15/2006

materials with similar lattice constants to avoid the formation of defects at the core−shell interface. In this structure, the distance between the luminescent lanthanide ions and the surface quenchers is increased, thus reducing the nonradiative pathways and increasing the quantum yield of nanomaterials.

In comparison with the conventional oxide-based luminescent materials, fluorides are advantageous as fluorescent host materials owing to their low vibrational energies, and the subsequent minimization of the quenching of the excited state of the rare-earth ions.[10] Hence, nanoparticles of fluoride materials have attracted a lot of interest due to their potential applications in optics and optoelectronics (e.g., lighting and displays, optical amplifiers, lasers, up-converters, and scintillators).[11,12] As a potential scintillator and tunable laser material, CeF_3 is a luminescent material with 100% activator concentration.[13] A bulk crystal of CeF_3 possesses a hexagonal phase structure with a space group of $P\bar{3}c1$ (D_{3d}^4) and lattice constants $a = 0.713$ nm, $c = 0.729$ nm, and there are six molecules in the unit cell. The Ce^{3+} ion in the CeF_3 crystal is coordinated by nine F^- and has a C_2 site symmetry.[13b,c] Nanostructural CeF_3 materials have been prepared by a micromulsion method,[14] an electrospray technique,[11a] the thermolysis of single-source precursor in high-boiling solvents, and so forth.[10]

The polyol process was initially described for the preparation of elemental metals and alloys, in which the reducing properties of a high-boiling alcohol (e.g., glycerol, glycol) toward a suitable metal precursor were utilized.[15a,b] Later, it has been extensively used for the synthesis of nanoscale oxide, sulfide, and phosphate materials.[15c−e] Recently, S. Eiden-Assmann and G. Maret reported the synthesis of CeF_3 nanoparticles (5−10 nm in size) via the polyol process but failed to characterize their optical properties.[15f] Here we report the polyol synthesis and optical properties of fluoride nanocrystals: CeF_3, CeF_3:Tb^{3+}, and CeF_3:Tb^{3+}/LaF_3 (core/shell). The as-formed nanocrystals can be well-dispersed in ethanol to form clear colloidal solutions. The morphology, structure, luminescence, and energy transfer properties of these nanoparticles were investigated in detail in this paper.

II. Experimental Section

Synthesis. La_2O_3 (99.99%, Shanghai Yuelong New Materials Co., Ltd.), Tb_4O_7 (99.99%, Shanghai Yuelong New Materials Co., Ltd.), $Ce(NO_3)_3{\cdot}6H_2O$ (99.99%, Shanghai Yuelong New Materials Co., Ltd.), and NH_4F (96.0%, analytical reagent, A. R., Beijing Beihua Chemicals Co., Ltd.) were used as starting materials without any further purification. $La(NO_3)_3$ and $Tb(NO_3)_3$ were prepared by dissolving the corresponding oxides in diluted nitric acid, and the water in the solutions was distilled off by heating.

CeF_3 Nanoparticles. A 2 mmol portion of $Ce(NO_3)_3{\cdot}6H_2O$ was dissolved in 25 mL of diethylene glycol (DEG, 98.0%, A. R.) in a round-bottomed flask at 100 °C under stirring to form a clear solution. The solution was then heated in a silicon oil bath under vigorous stirring with a flow of Ar atmosphere, and the temperature of the solution was further increased to 200 °C. At this temperature, a solution of DEG (25 mL) containing 6 mmol of NH_4F was injected into the above solution, and the mixture was kept at 200 °C for 1 h. Then, the obtained suspension was cooled to room temperature and diluted with 50 mL of ethanol. The solid particles were separated by centrifugation at a speed of 4500 rpm. To remove residual DEG, the solid powders were dispersed in ethanol and centrifuged again. The final solid sample could be easily redispersed in ethanol to form transparent colloidal solution.

CeF_3: Tb^{3+} Nanoparticles. The doping concentration of Tb^{3+} in CeF_3 host varied from 0.1 to 30 mol %. Stoichiometric amounts of $Ce(NO_3)_3{\cdot}6H_2O$ and $Tb(NO_3)_3$ (totally 2.0 mmol) were dissolved in 25 mL of DEG at 100 °C under stirring to form a clear solution. The other procedures were same as those for the synthesis of CeF_3 nanoparticles as elucidated above.

CeF_3:Tb^{3+}/LaF_3 (Core/Shell) Nanoparticles. The $Ce_{0.85}Tb_{0.15}F_3$/LaF_3 (core/shell) nanoparticles were prepared by a two-step process. Typically, 0.5 mmol of $La(NO_3)_3$ was dissolved in 12.5 mL of DEG at 100 °C under stirring to form a clear solution. Then, 25 mL of a DEG suspension of $Ce_{0.85}Tb_{0.15}F_3$ prepared above was added to the clear solution, and the mixed system was heated to 200 °C in a silicon oil bath under vigorous stirring with a flow of Ar. At this temperature, a solution of DEG (12.5 mL) containing 1.5 mmol of NH_4F was injected into the mixed system, and the suspension was kept at 200 °C for 1 h. The following procedures were same as those for the synthesis of CeF_3 nanoparticles as stated above.

Characterization. X-ray diffraction (XRD) was carried out on a Rigaku-Dmax 2500 diffractometer with Cu Kα radiation ($\lambda = 0.15405$ nm). The accelerating voltage and emission current were 40 kV and 200 mA, respectively. The specimens for the XRD test were prepared by putting quartz slits in the particle dispersion of ethanol, and the solvent was evaporated at room temperature. TEM images were obtained using a JEOL 2010 transmission electron microscope operating at 200 kV. Samples for TEM were prepared by depositing a drop of a colloidal ethanol solution of the powder sample onto a carbon coated copper grid. The excess liquid was wicked away with filter paper, and the grid was dried in air. The X-ray photoelectron spectra (XPS) were taken on a VG ESCALAB MK II electron energy spectrometer using Mg Kα (1253.6 eV) as the X-ray excitation source. The UV−Vis absorption spectra were measured on a TU-1901 spectrophotometer. The excitation and emission spectra were taken on an F-4500 spectrophotometer equipped with a 150 W xenon lamp as the excitation source. The luminescence lifetimes of Ce^{3+} and Tb^{3+} were measured with a Lecroy Wave Runner 6100 digital oscilloscope (1 GHz) using a 266 nm laser wavelength (pulse width = 4 ns) from YAG:Nd as

(10) Zhang, Y. W.; Sun, X.; Si, R.; You, L. P.; Yan, C. H. *J. Am. Chem. Soc.* **2005**, *127*, 3260−3261.
(11) (a) Cárcer, I. A.; Herrero, P.; Landa-Cánovas, A. R.; Sobolev, B. *Appl. Phys. Lett.* **2005**, *87*, 053105−1. (b) Stouwdam, J. W.; van Veggel, F. C. J. M. *Nano Lett.* **2002**, *2*, 733−737. (c) Yan, R.; Li, Y. *Adv. Funct. Mater.* **2005**, *15*, 763−769. (d) Heer, S.; Kömpe, K.; Güdel, H. U.; Haase, M. *Adv. Mater.* **2004**, *16*, 2102−2105. (e) Shimamura, K.; Víllora, E. G.; Nakakita, S.; Nikl, M.; Ichinose, N. *J. Cryst. Growth* **2004**, *264*, 208−215. (f) Yi, G. S.; Chow, G. M. *J. Mater. Chem.* **2005**, *15*, 4460−4464. (g) Lemyre, J. L.; Ritcey, A. M. *Chem. Mater.* **2005**, *17*, 3040−3043. (h) Yi, G.; Lu, H.; Zhao, S.; Ge, Y.; Yang, W.; Chen, D.; Guo, L. H. *Nano Lett.* **2004**, *4*, 2191−2196.
(12) Fang, Y. C.; Zhang, Z. J.; Xie, Z. Q.; Zhao, Y. Y.; Lu, M. *Appl. Phys. Lett.* **2005**, *86*, 191919-1.
(13) (a) Blasse, G.; Grabmaier, B. C. *Luminescent Materials*; Springer: Berlin, 1994. (b) Wojtowicz, A. J.; Balcerzyk, M.; Berman, E.; Lempicki, A. *Phys. Rev. B* **1994**, *49*, 14880−14894.(c) Wei, K.; Guo, C. X.; Deng, J.; Shi, C. S. *J. Elec. Spectrosc. Related Phenom. A* **1996**, *79*, 83−85.
(14) (a) Qiu, S.; Dong, J.; Chen, G. *Powder Technol.* **2000**, *113*, 9−13. (b) Lian, H.; Zhang, M.; Liu, J.; Ye, Z.; Yan, J.; Shi, C. *Chem. Phys. Lett.* **2004**, *395*, 362−365.
(15) (a) Deschamps, A.; Lagier, J. P.; Fievet, F.; Aeiyach, S.; Lacaze, P. C. *J. Mater. Chem.* **1992**, *2*, 1213−1214. (b) Toneguzzo, P.; Acher, O.; Viau, G.; Pierrard, A.; Fievet-Vincent, F.; Fievet, F.; Rosenman, I. *IEEE Trans. Magnet.* **1999**, *35*, 3469−3471. (c) Feldmann, C.; Jungk, H.-O. *Angew. Chem., Int. Ed.* **2001**, *40*, 359−362. (d) Feldmann, C. *Solid State Sci.* **2005**, *7*, 868−873. (e) Feldmann, C. *Adv. Funct. Mater.* **2003**, *13*, 101−107. (f) Eiden-Assmann, S.; Maret, G. *Mater. Res. Bull.* **2004**, *39*, 21−24.

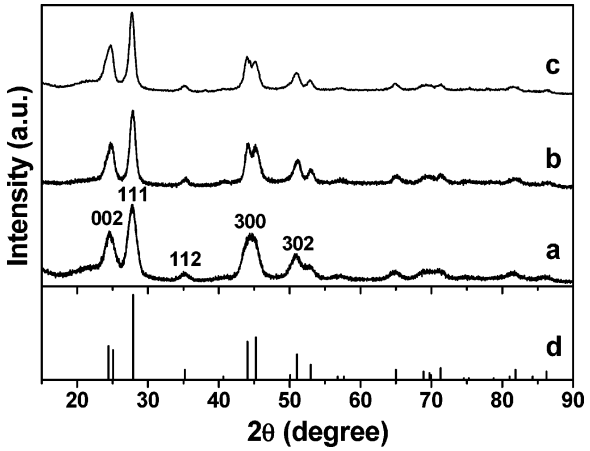

Figure 1. XRD patterns of CeF_3 (a), $Ce_{0.85}Tb_{0.15}F_3$ (b), and $Ce_{0.85}Tb_{0.15}F_3/LaF_3$ core/shell (c) nanoparticles and the standard data for CeF_3 (d) (JCPDS Card 08-0045).

Table 1. Calculated Crystal Cell Parameters and Average Size of CeF_3, $Ce_{0.85}Tb_{0.15}F_3$, and $Ce_{0.85}Tb_{0.15}F_3/LaF_3$ Core/Shell Nanoparticles

	cryst cell params (nm)		av particle size (nm)	
	a	*c*	XRD	TEM
CeF_3	0.7132	0.7264	8.0	7.5
$Ce_{0.85}Tb_{0.15}F_3$	0.7105	0.7264	8.5	7.0
$Ce_{0.85}Tb_{0.15}F_3/LaF_3$ core/shell	0.7108	0.7310	11.5	11.0

the excitation source. The spectra and lifetimes were obtained from the colloidal (ethanol) solutions of CeF_3, CeF_3:Tb^{3+}, and CeF_3:Tb^{3+}/LaF_3 nanoparticles with a concentration of 22.86 mmol/L. All the measurements were performed at room temperature.

III. Results and Discussion

Formation, Structure, and Morphology of the Nanocrystals. XRD. The phase structures of the nanoparticles were investigated by XRD. Figure 1 shows XRD patterns of CeF_3 (a), $Ce_{0.85}Tb_{0.15}F_3$ (b), and $Ce_{0.85}Tb_{0.15}F_3/LaF_3$ core/shell (c) nanoparticles and the standard data for CeF_3 (d) as well. The results of the XRD indicate that these three samples crystallized well, and the patterns are in good agreement with hexagonal phase structure known from the bulk CeF_3 crystal (JCPDS Card 08-0045). For the InAs/InP core/shell system, with the growth of the InP shell, the diffraction peaks shift to larger angles because of the smaller lattice constant for InP compared with InAs.[8b] However, for our CeF_3:Tb^{3+}/LaF_3 core/shell system, no obvious shift is observed for the diffraction peaks with respect to those of the CeF_3:Tb^{3+} core nanoparticles (as shown in Figure 1), which is due to the similar lattice constants between LaF_3 and CeF_3. The crystal cell parameters of the three samples calculated according to their XRD data are listed in Table 1, which are in good agreement with the reported values for bulk CeF_3 crystals ($a = 0.713$ nm, $c = 0.729$ nm).[13b] In Figure 1, the diffraction peaks for three samples are broadened due to the smaller crystallite size. The crystallite size can be estimated from the Scherrer equation, $D = 0.90\lambda/\beta \cos \theta$, where D is the average grain size, λ is the X-ray wavelength (0.15405 nm), and θ and β are the diffraction angle and full-width at half-maximum (fwhm) of an observed peak, respectively.[16] The strongest peak (111) at $2\theta = 27.8°$ was used to calculate the average crystallite size (D) of these nanoparticles. The estimated average crystallite sizes of CeF_3, $Ce_{0.85}Tb_{0.15}F_3$, and $Ce_{0.85}Tb_{0.15}F_3/LaF_3$ core/shell nanoparticles are around 8, 8.5, and 11.5 nm, respectively, as shown in Table 1.

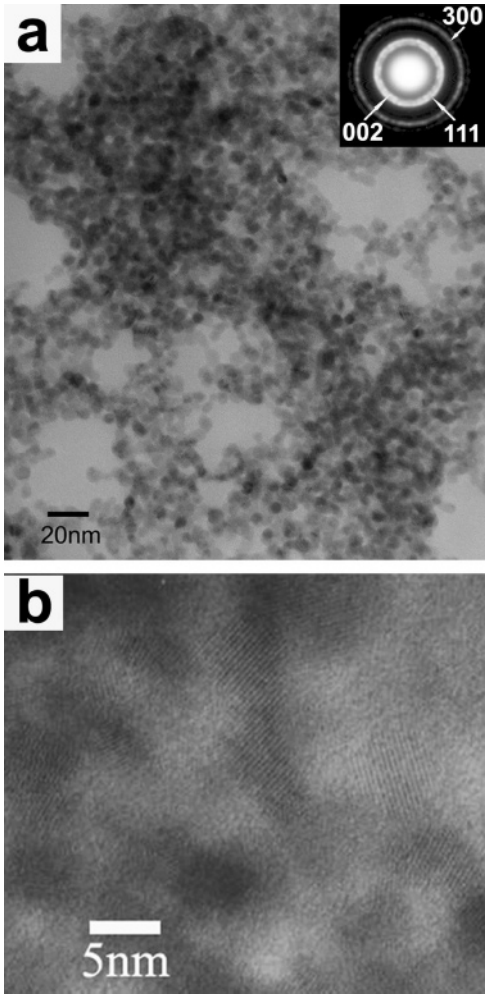

Figure 2. Low-resolution (a) and high-resolution (b) TEM images of CeF_3 nanoparticles. The inset is a selected area electron diffraction pattern (SAED).

TEM. CeF_3 nanoparticles with a relatively narrow particle size distribution can be prepared via the polyol process.[15f] Figure 2 shows the low-resolution (a) and high-resolution (b) TEM images of CeF_3 nanoparticles. The low-resolution TEM image illustrates that the well-separated CeF_3 nanoparticles are almost spherical with a mean diameter of 7 nm, which is basically consistent with the calculated value using the Scherrer equation. This demonstrates that all the nanoparticles are single crystals, which can be further confirmed by the high-resolution TEM micrographs. The high degree of dispersibility may indicate that the surface of the nuclei is covered by polyol medium right after formation, which limits the growth of particles and stabilizes them against agglomeration.[15] The high-resolution transmission electron micrograph (HRTEM) image given in Figure 2b displays lattice fringes for nanoparticles, indicating that these CeF_3 nanoparticles possess high crystallinity. The selected area electron diffraction (SAED) patterns are consistent with a

(16) Zhang, Y. W.; Yang, Y.; Jin, S.; Tian, S. J.; Li, G. B.; Jia, J. T.; Liao, C. S.; Yan, C. H. *Chem. Mater.* **2001**, *13*, 372−378.

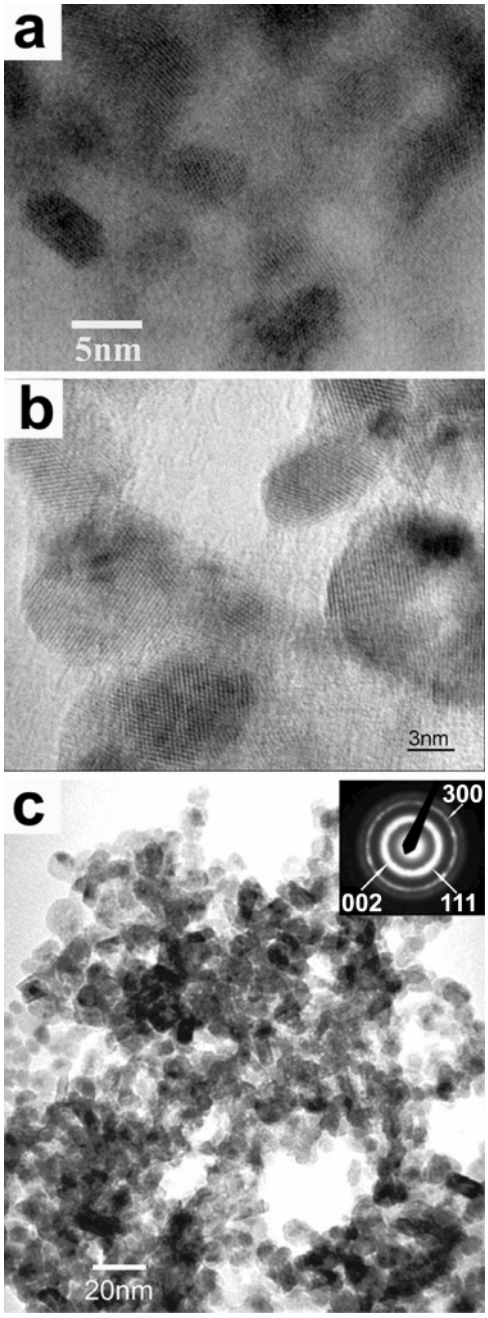

Figure 3. High-resolution TEM images of $Ce_{0.85}Tb_{0.15}F_3$ nanoparticles before (a) and after (b) growth of the LaF_3 shell as well as low-resolution TEM image of $Ce_{0.85}Tb_{0.15}F_3/LaF_3$ core/shell nanoparticles (c) (Inset is a selected area electron diffraction pattern, SAED.)

hexagonal phase structure of CeF_3 with strong ring patterns due to (002), (111), and (300) planes (Figure 2, inset), in good agreement with XRD patterns. The average size, the SAED patterns, and the morphology of CeF_3:Tb^{3+} particles are almost identical with those of CeF_3, indicating that the dopant ion Tb^{3+} has little effect on the morphology and crystallinity of CeF_3. In other words, we can say that the Tb^{3+} ions are well-dissolved in CeF_3 nanocrystals. The HRTEM image (Figure 3a) for $Ce_{0.85}Tb_{0.15}F_3$ particles clearly revealed the well-resolved diffraction fringes of the particle lattices, indicating that these nanoparticles are also highly crystalline. Figure 3b,c shows the high-resolution and low-resolution TEM images of $Ce_{0.85}Tb_{0.15}F_3/LaF_3$ core/shell nanoparticles, respectively. It is clearly observed that the

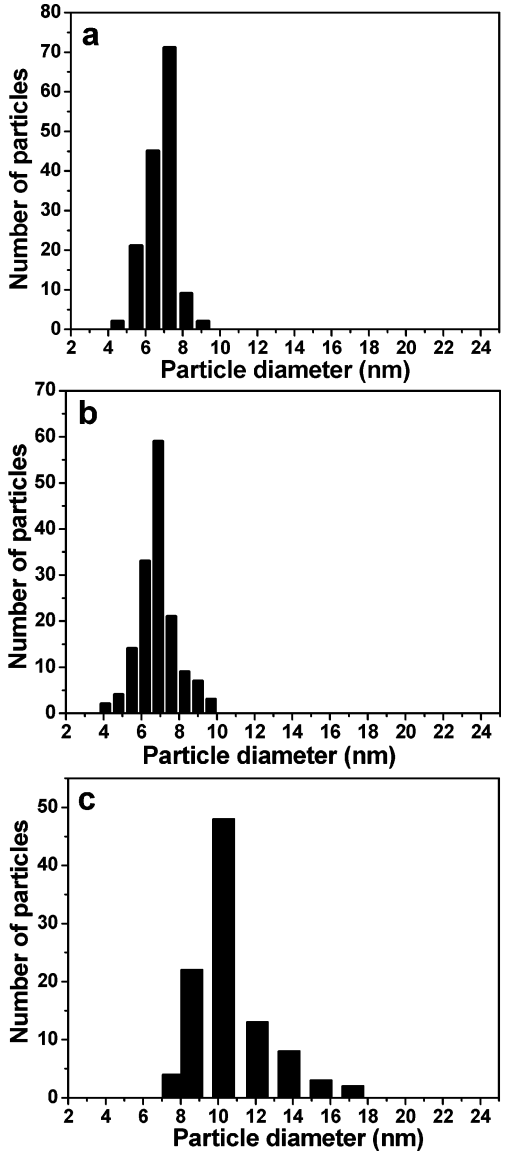

Figure 4. Particle size distribution histograms of CeF_3 (a), $Ce_{0.85}Tb_{0.15}F_3$ (b), and $Ce_{0.85}Tb_{0.15}F_3/LaF_3$ core/shell (c) nanoparticles measured from TEM images.

growth of the shell layers resulted in an increase of the average size of the nanopaticles as well as a broadening of their size distribution. The average particle diameter increases from 7 nm for the spherical $Ce_{0.85}Tb_{0.15}F_3$ core particles to 11 nm for the slightly elongated $Ce_{0.85}Tb_{0.15}F_3/LaF_3$ core/shell particles. The average diameters of these three samples determined by TEM images and calculated by XRD data are collected in Table 1. The estimated average thickness of LaF_3 shells on CeF_3:Tb^{3+} cores is about 2 nm [$(11 - 7)/2 = 2$ (nm)] assuming that the particles are in spherical shape. In TEM images, contrast depends on the electron scattering power of the object forming the images. The electron scattering power in turn depends on the electron density inside the object.[4a] Hence, direct evidence can be obtained from the image contrast for the core/shell structure with different lattice parameters. The core and the shell of the nanoparticles, however, have similar electron density and lattice parameters, and the image contrast cannot be used to distinguish the shell and core. The SAED patterns (Figure 3, inset) are the same as those of CeF_3 nanoparticles, which

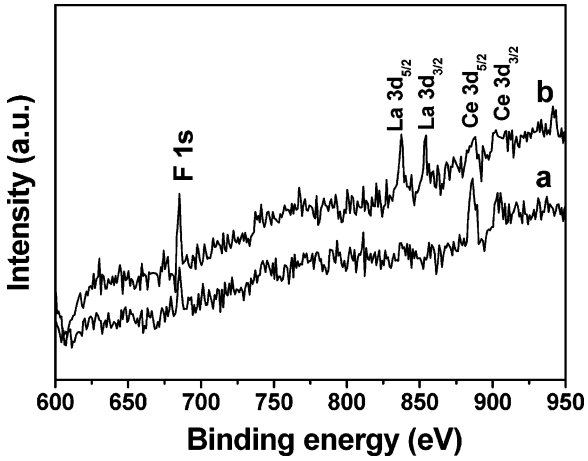

Figure 5. XPS spectra of $Ce_{0.85}Tb_{0.15}F_3$ (a) and $Ce_{0.85}Tb_{0.15}F_3/LaF_3$ core/shell (b) nanoparticles.

is in good agreement with XRD patterns. High crystallinity is also inferred from the high-resolution TEM images which show the lattice fringes for most particles. Figure 4 shows the particle size distribution histograms of CeF_3 (a), $Ce_{0.85}Tb_{0.15}F_3$ (b), and $Ce_{0.85}Tb_{0.15}F_3/LaF_3$ core/shell (c) nanoparticles. Size distributions were obtained by counting particle size on a minimum of 100 nanoparticles (the sizes of the elongated particles were determined by averaging of the long and the short axes). It can be seen that the size distributions of CeF_3 and $CeF_3:Tb^{3+}$ nanoparticles are similar (Figure 4a,b), which are narrower than that (Figure 4c) of the $Ce_{0.85}Tb_{0.15}F_3/LaF_3$ core/shell nanoparticles.

XPS. To further confirm the growth of the LaF_3 shells around the $CeF_3:Tb^{3+}$ core nanoparticles, the $CeF_3:Tb^{3+}$ and $CeF_3:Tb^{3+}/LaF_3$ core/shell nanoparticles were subjected to XPS analysis. Figure 5 shows the XPS spectra of $Ce_{0.85}Tb_{0.15}F_3$ core (a) and $Ce_{0.85}Tb_{0.15}F_3/LaF_3$ core/shell (b) nanoparticles. The binding energies at 886.1 and 903.3 eV in Figure 5a are attributed to Ce $3d_{5/2}$ and $3d_{3/2}$ peaks, respectively.[17] When the shell of LaF_3 was grown onto the core of $CeF_3:Tb^{3+}$ nanoparticles to form the core/shell structure, the Ce $3d_{5/2}$ and $3d_{3/2}$ peaks dropped strongly and the La peaks at 837.1 ($3d_{5/2}$) and 854.2 eV ($3d_{3/2}$) dominated in the spectrum,[2a] as shown in Figure 5b. This is consistent with the proposed structure where LaF_3 is the shell that encapsulates the $CeF_3:Tb^{3+}$ core.

Photoluminescent Properties. Spectral Properties. The as-formed CeF_3, $CeF_3:Tb^{3+}$, and $CeF_3:Tb^{3+}/LaF_3$ (core/shell) nanoparticles can be well-dispersed in ethanol to form transparent colloidal solutions. Under 254 nm UV lamp irradiation, the colloidal solutions exhibit purple-blue (CeF_3) and bright green emission ($CeF_3:Tb^{3+}$ and $CeF_3:Tb^{3+}/LaF_3$), respectively, as shown in Figure 6 (all three solutions have the same concentration, 22.86 mmol/L).

Figure 7 gives the excitation (a), emission (b), and UV−vis absorption (c) spectra of dilute ethanol solution of CeF_3 nanoparticles. The emission spectrum (Figure 7b) of CeF_3 nanoparticles includes a broad band ranging from 290 to 400 nm peaking at 320 nm (CIE color coordinate $x = 0.156$, $y = 0.030$), which can be attributed to the 5d−4f transition of

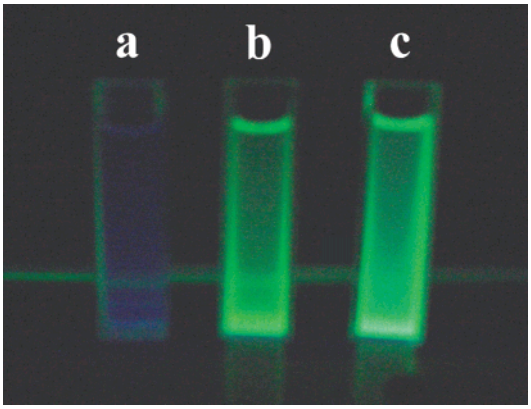

Figure 6. Photographs of dispersions of CeF_3 (a), $Ce_{0.85}Tb_{0.15}F_3$ (b), and $Ce_{0.85}Tb_{0.15}F_3/LaF_3$ core/shell (c) nanoparticles in dilute ethanol solution under irradiation of a 254 nm UV lamp.

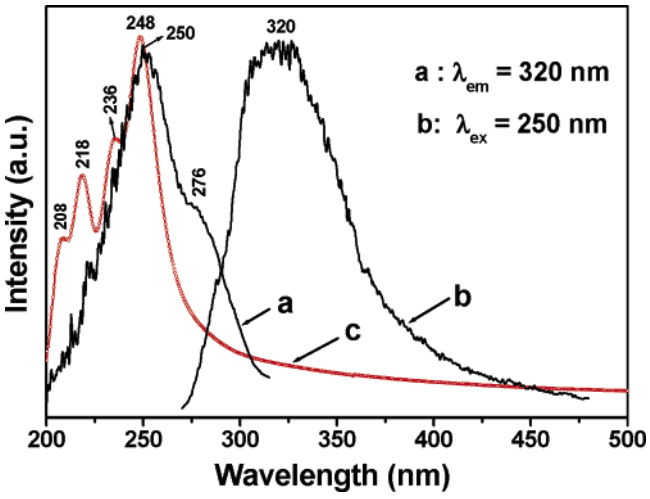

Figure 7. Excitation (a), emission (b), and UV−vis absorption (c) spectra of dilute ethanol solutions of CeF_3 nanoparticles.

Ce^{3+}.[13b,13c,14b] Note that in a thin film[18] and the bulk[19] of $LaPO_4:Ce^{3+}$, two well-resolved emission peaks at 318 and 336 nm are observed due to the ground-state splitting of Ce^{3+} ($^2F_{5/2}$, $^2F_{7/2}$). This splitting for Ce^{3+} in the current CeF_3 nanoparticles cannot be resolved clearly due to the broadening of spectral lines induced by the small size effects. Monitored with the emission wavelength of 320 nm, the obtained excitation spectrum (Figure 6a) consists of a broad and strong band with a maximum at 250 nm and a shoulder at 276 nm, which correspond to the transitions from the ground state $^2F_{5/2}$ of Ce^{3+} to the different components of the excited Ce^{3+} 5d states split by the crystal field.[18] The UV−vis absorption spectrum (Figure 6c) of CeF_3 nanoparticles dispersed in ethanol solution shows four well-resolved absorption peaks at 248, 236, 218, and 208 nm for the Ce^{3+}, basically in agreement with the excitation spectrum (note that the peaks at 236, 218, and 208 nm also seem to exist in the excitation spectrum of Figure 7a evidenced by the stronger noise signals there). The Stokes shift for the luminescence of Ce^{3+} in CeF_3 nanocrystals amounts to 9000 cm^{-1}, a pretty large value. The above spectral properties (excitation, absorption, and emission spectra) of CeF_3 nanoc-

(17) Pemba-Mabiala, J. M.; Lenzi, M.; Lenzi, J. Lebugle, A. *Surf. Interface Anal.* **1990**, *15*, 663.

(18) Yu, M.; Lin, J.; Fu, J.; Zhang, H. J.; Han, Y. C. *J. Mater. Chem.* **2003**, *13*, 1413−1419.

(19) Blasse, G.; Bril, A. *J. Chem. Phys.* **1969**, *51*, 3252−3254.

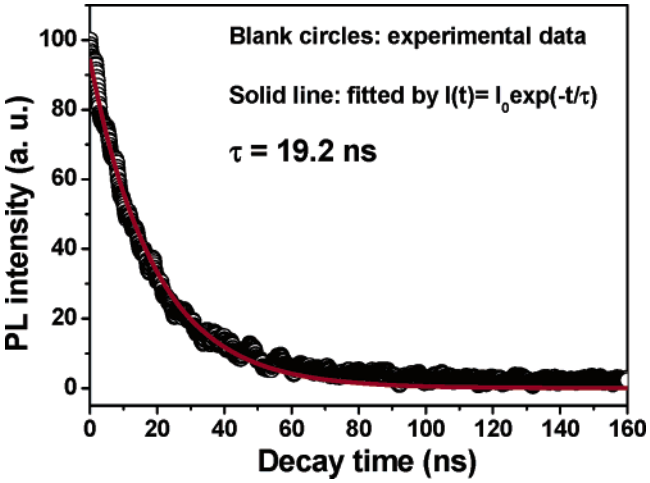

Figure 8. Decay curve of Ce^{3+} luminescence (320 nm) in dilute ethanol solution of CeF_3 nanoparticles (λ_{ex} = 266 nm).

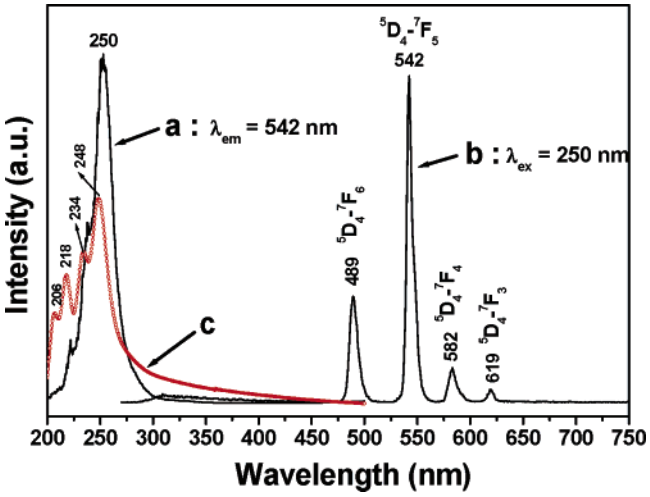

Figure 9. Excitation (a), emission (b), and UV−vis absorption (c) spectra of dilute ethanol solutions of $Ce_{0.85}Tb_{0.15}F_3$ nanoparticles.

rystals are basically consistent with those reported for the CeF_3 bulk crystals.[13b,c] CeF_3, which shows quite strong emission at room temperature, is a luminescent material with 100% activator concentration.[13] This can be attributed to two factors in this compound. On one hand, a smaller spectral overlap (i.e., larger Stokes shift, 9000 cm^{-1}) prevents resonant energy migration among the Ce^{3+} ions, thus decreasing the probability of concentration quenching by energy migration. On the other hand, although at room temperature phonon-assisted energy transfer among the Ce^{3+} ions might occur and compete with 5d−4f transition (in Ce^{3+}) and vibronic relaxation, the latter is very efficient because of the electric dipole allowed the d−f transition and strong vibronic coupling.[13b] Consequently, the emission of CeF_3 is not quenched at room temperature.

Figure 8 shows the luminescence decay curve of Ce^{3+} in CeF_3 nanoparticles. This curve can be well-fit into a single-exponential function as $I = I_0 \exp(-t/\tau)$ (τ is 1/*e* lifetime of the Ce^{3+} ion). The lifetime of Ce^{3+} is determined to be 19.2 ns, a value which is in good agreement with the reported lifetimes of Ce^{3+}.[13b,20a] The short lifetime of Ce^{3+} is due to the allowed character for its 5d−4f transition.

The CeF_3 nanoparticles doped with a Tb^{3+} ion show a strong green emission under UV excitation. Figure 9 gives the excitation (a), emission (b), and absorption (c) spectra of $Ce_{0.85}Tb_{0.15}F_3$ nanoparticles in dilute ethanol solutions. The excitation spectrum (Figure 9a) monitored with the 542 nm emission ($^5D_4-^7F_5$) of Tb^{3+} is identical to that of CeF_3 nanoparticles (Figure 7a). The absorption spectrum (Figure 9c) of $Ce_{0.85}Tb_{0.15}F_3$ nanoparticles dispersed in ethanol solution shows four absorption peaks at 248, 234, 218, and 206 nm for the Ce^{3+}, agreeing well with that of CeF_3 nanoparticles (Figure 7c). Excitation into the Ce^{3+} band at 250 nm yields both the weak emission of Ce^{3+} (300−400 nm) and strong emission of Tb^{3+} (450−650 nm) (CIE color coordinate x = 0.261, y =0.614). This indicates that an energy transfer from Ce^{3+} to Tb^{3+} occurs in the CeF_3:Tb^{3+} nanoparticles, as observed in the bulk powder materials [20b] and colloids of

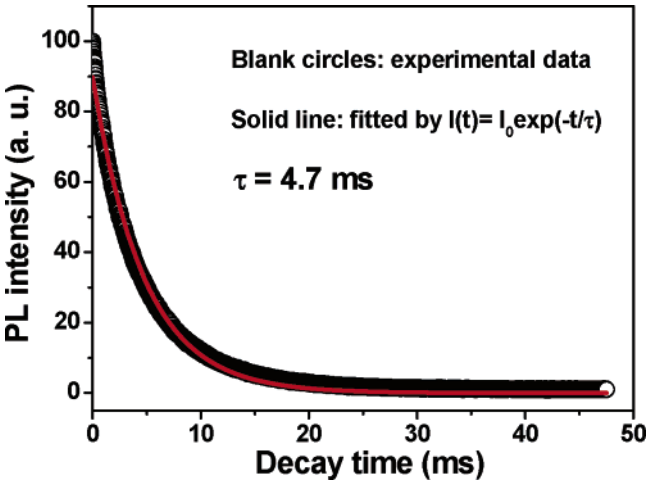

Figure 10. Decay curve of Tb^{3+} luminescence (542 nm) in dilute ethanol solution of $Ce_{0.85}Tb_{0.15}F_3$ nanoparticles (λ_{ex} = 266 nm).

$LaPO_4$:Ce^{3+}, Tb^{3+}.[21] The emission of Tb^{3+} is due to transitions between the excited $^5D_4$ state and the ^7F_J (J = 6−3) ground states of Tb^{3+} ions. No emission from the higher $^5D_3$ level is observed due to a cross relaxation effect at the high Tb^{3+} concentration.[18] Figure 10 shows the luminescence decay curve of Tb^{3+} in $Ce_{0.85}Tb_{0.15}F_3$ nanoparticle ethanol solution. This decay curve of Tb^{3+} can also be fitted into a single-exponential function as $I = I_0 \exp(-t/\tau)$ (τ is 1/*e* lifetime of the Tb^{3+} ion). The lifetime of Tb^{3+} is determined to be 4.7 ms in $Ce_{0.85}Tb_{0.15}F_3$ nanoparticles.

The emission intensity of CeF_3:Tb^{3+} nanoparticles is affected by the Tb^{3+}-doped concentration. The effect of Tb^{3+} concentration (x) on the emission intensities of $Ce_{1-x}Tb_xF_3$ nanoparticles is shown in Figure 11. It can be seen from this figure that, with increasing Tb^{3+} concentration, the intensity increases gradually and reaches the maxmum at x = 0.15 (15 mol %), and then decreases. The decrease in emission intensity is due to the concentration quenching

(20) (a) Yoshikawa, A.; Satonaga, T.; Kamada, K.; Sato, H.; Nikl, M.; Solovieva, N.; Fukuda, T. *J. Cryst. Growth* **2004**, *270*, 427−432. (b) Bourcet, J. C.; Fong, F. K. *J. Chem. Phys.* **1974**, *60*, 34−39.

(21) (a) Riwotzki, K.; Meyssamy, H.; Schnablegger, H.; Kornowski, A.; Haase, M. *Angew. Chem., Int. Ed.* **2001**, *40*, 573−576. (b) Riwotzki, K.; Meyssamy, H.; Kornowski, A.; Haase, M. *J. Phys. Chem. B* **2000**, *104*, 2824−2828.

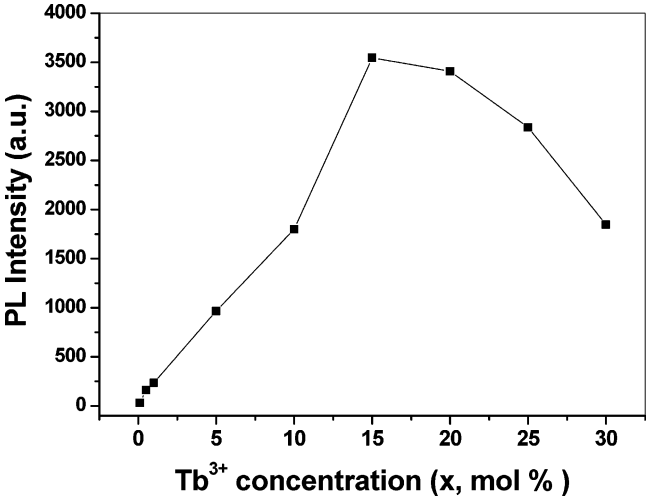

Figure 11. Effect of Tb^{3+} concentration (x) on the emission intensity of $Ce_{1-x}Tb_xF_3$ nanoparticles in dilute ethanol solutions.

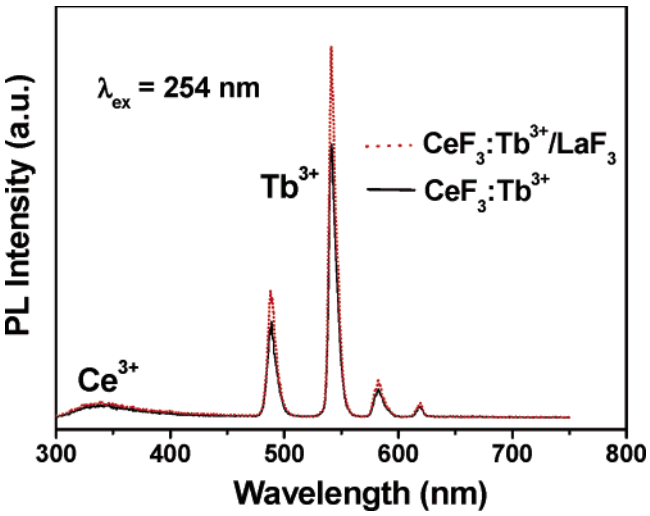

Figure 12. Emission spectra of $Ce_{0.85}Tb_{0.15}F_3$ (solid line) and $Ce_{0.85}Tb_{0.15}F_3/LaF_3$ core/shell (dotted line) nanoparticles in dilute ethanol solutions.

effect at higher Tb^{3+} doping concentration. This effect of Tb^{3+} doping concentrations on luminescence intensities in CeF_3:Tb^{3+} nanoparticles is similar to what we have observed in the nanocrystalline $LaPO_4$:Ce^{3+}, Tb^{3+} films.[18]

Figure 12 shows the emission spectra of $Ce_{0.85}Tb_{0.15}F_3$ (solid line) and $Ce_{0.85}Tb_{0.15}F_3/LaF_3$ core/shell (dotted line) nanoparticles in dilute ethanol solutions. The spectra of $Ce_{0.85}Tb_{0.15}F_3$ and $Ce_{0.85}Tb_{0.15}F_3/LaF_3$ core/shell nanoparticles are similar in profile (both consisting of the characteristic emission of Tb^{3+} with the $^5D_4-^7F_5$ transition at 542 nm being the most prominent group). When the CeF_3:Tb^{3+} nanoparticles were coated with the LaF_3 shells, the emission intensity was improved by 40% with respect to that of CeF_3:Tb^{3+} core particles. We believe that this is a relatively big enhancement for the luminescence of nanophosphors which generally have a low emission intensity. This increase of emission intensity may be attributed to the fact that a significant amount of nonradiative centers existing on the surface of CeF_3:Tb^{3+} nanoparticles are eliminated by the shielding effect of the LaF_3 shell.[2a] In this core/shell structure, the distance between the luminescent lanthanide ions and the surface quenchers is increased, thus reducing the nonradiative pathways and

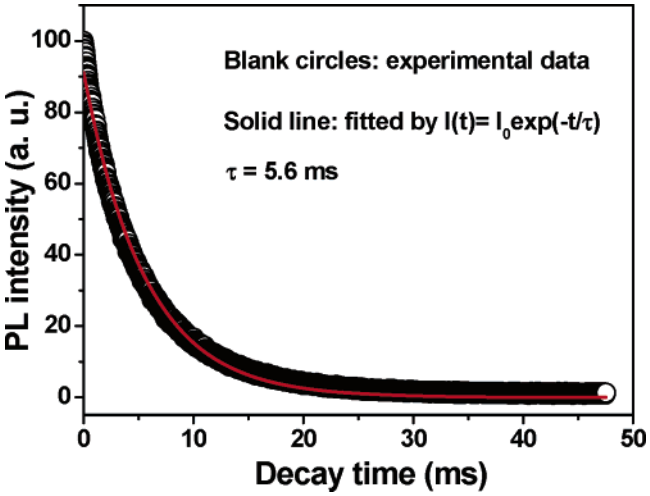

Figure 13. Decay curve of Tb^{3+} luminescence (542 nm) in $Ce_{0.85}Tb_{0.15}F_3/LaF_3$ core/shell nanoparticles (λ_{ex} = 266 nm).

suppressing the energy quenching in energy-transfer precesses. In addition, the enhanced emission intensity may further result from the suppression of solvent quenching by the LaF_3 shell. The C−H and O−H vibrations of the solvent can quench surface luminescent centers of CeF_3:Tb^{3+} nanoparticles. When the LaF_3 shell was grown around the surface of CeF_3:Tb^{3+} nanoparticles, the surface luminescent centers were protected from the solvents.[2a]

The luminescence decay curve of Tb^{3+} in $Ce_{0.85}Tb_{0.15}F_3/LaF_3$ core/shell nanoparticles can be also fitted into a single-exponential function, and the lifetime of Tb^{3+} is determined to be 5.6 ms, as shown in Figure 13. The increase of the luminescence lifetime for Tb^{3+} in $Ce_{0.85}Tb_{0.15}F_3/LaF_3$ core/shell nanoparticles with respect to that (4.7 ms) in $Ce_{0.85}Tb_{0.15}F_3$ core nanoparticles indicates that quenching from outside the particles is strongly reduced after the growth of a shell around the core. This is additional evidence for the formation of core/shell structure. The effect of the core/shell structure on the quenching from outside of the particles can be interpreted with the model of the luminescence decay proposed by van Veggel and co-workers.[1b,9c] According to this model, the luminescence decay can be expressed by the following equation:

$$I_t = I_0 \sum_{i=1}^{n} \frac{1}{n} e^{-kit};\ k_i = \frac{1}{\tau_i} = k_R + C \times f_{q,i}$$

where I_0 is the normalized intensity at time $t = 0$, n is the number of shells, $k_i = 1/\tau_i$, is the rate constant for the ith shell, $k_R = 1/\tau_R$ is the rate constant in the absence of quenching from outside particles. The factor $f_{q,i}$ is the relative quenching factor, and C is the quenching constant. The $f_{q,i}$ values depend on the distance of a shell to the surface. The constant C is a fit parameter that is dependent on the individual ion, on the size and size distribution of the particles, and on the strength of the quenching.[9c] When quenching is assumed to take place via a dipole−dipole mechanism, the quenching has a distance dependence of r^{-6}, where r is the distance between the quenching moiety and the excited lanthanide ion (Ln^{3+}), so major quenching occurs at or near the surface of the particles and the growth of a

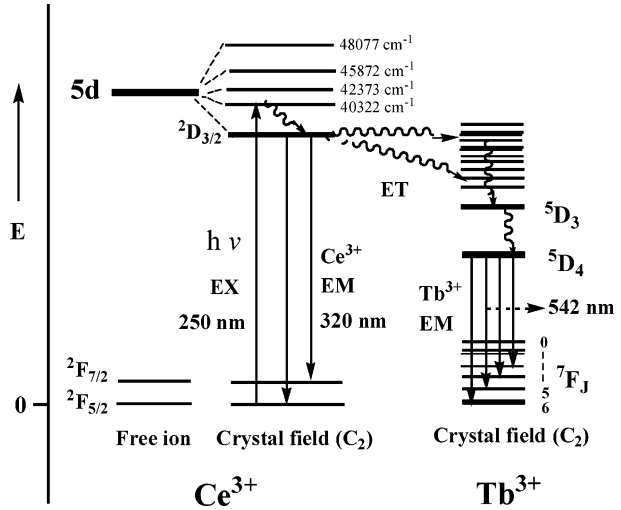

Figure 14. Energy level scheme of CeF_3:Tb^{3+} with electronic transitions and energy transfer processes.

Table 2. The Lifetime (τ) of Ce^{3+} in $Ce_{1-x}Tb_xF_3$ ($x = 0-0.20$) Nanoparticles (Colloidal Solution of Ethanol) upon Excitation into the Ce^{3+} with 266 nm Laser

	$x = 0$	$x = 0.05$	$x = 0.10$	$x = 0.15$	$x = 0.20$
$\tau(Ce^{3+})$ (ns)	19.2	19.0	18.4	16.5	14.1

shell around the luminescent core can reduce the quenching. This model has been successfully applied to explain the changes of the lifetimes of luminescent trivalent lanthanide ions (Eu^{3+}, Nd^{3+}, Er^{3+}, Pr^{3+}, Ho^{3+}, and Yb^{3+})-doped LaF_3 and $LaPO_4$ nanoparticles coated with different organic ligands.[1b,9c]

Energy Transfer. Energy transfer plays an important role in improving the emission efficiency for solid-state luminescent materials. Electronic transitions within $4f^n$ configurations of Tb^{3+} are so strongly forbidden that they appear in the absorption spectra with very weak intensity. However, excitation resulting in high light output can be achieved by exciting a different ion (sensitizer, i.e., Ce^{3+}) with an allowed electronic transition which transfers the excitation energy to the rare earth activator (i.e., Tb^{3+}). So, the energy transfer processes from Ce^{3+} to Tb^{3+} can enhance the Tb^{3+} green emission in CeF_3:Tb^{3+} nanoparticles. To confirm the energy transfer process from Ce^{3+} to Tb^{3+} further, the lifetimes of Ce^{3+} in the colloidal solution of $Ce_{1-x}Tb_xF_3$ ($x = 0-0.20$) nanoparticles were measured, as collected in Table 2. The Ce^{3+} lifetime (τ) decreases with increasing the Tb^{3+} concentrations, which indicates that an energy transfer from Ce^{3+} to Tb^{3+} occurs in the CeF_3:Tb^{3+} nanoparticles.[18,20,22]

The energy transfer phenomenon from Ce^{3+} to Tb^{3+} has been observed in quite a few host lattices.[19,20b,21a,22] The energy levels of Tb^{3+} are suitable for energy transfer to take place from the allowed Ce^{3+} emission of (f−d) upon excitation with UV light. In the CeF_3 system, almost no $Ce^{3+}-Ce^{3+}$ energy transfer occurs,[13] so first Ce^{3+} ions were excited by UV light excitation; subsequently energy transfer takes place from Ce^{3+} to Tb^{3+} ions.[19] The energy level scheme of CeF_3:Tb^{3+} with electronic transitions (Ce^{3+}, Tb^{3+}) and energy transfer processes ($Ce^{3+}-Tb^{3+}$) is schematically shown in Figure 14.[20b,21a] Critical distance (R_c) is thought to be an important parameter in energy transfer, so we calculated R_c in $Ce_{0.85}Tb_{0.15}F_3$ nanoparticles. The excitation spectrum of Tb^{3+}, composed of several narrow lines (Tb^{3+} f−f transitions located from 26 400 to 35 200 cm^{-1}), was obtained from the literature.[23a] Considering the electric dipole−dipole interaction, $R_c^6 = 0.6 \times 10^{28} \times 4.8 \times 10^{-16} \times f_A \times E^{-4} \times SO$, where oscillator strength f_A (Tb^{3+}) = 10^{-6} (spin forbidden narrow line transitions of Tb^{3+}), E = 3.8409 eV (the energy of maximum spectral overlap), and SO = 0.7288 eV^{-1} (the normalized spectral overlap between the excitation lines of Tb^{3+} and the emission of Ce^{3+}), we arrive at R_c = 0.46 nm in $Ce_{0.85}Tb_{0.15}F_3$ nanoparticles.[23b-d] Athough this critical distance value is not very accurate, it indicates that the energy transfer occurs mainly between nearest neighbors of Ce^{3+} and Tb^{3+}.

IV. Conclusions

Well-crystallized CeF_3, CeF_3:Tb^{3+}, and CeF_3:Tb^{3+}/LaF_3 (core/shell) nanoparticles have been successfully prepared by a polyol process. These nanoparticles, ranging from 7 to 11 nm, with nearly spherical morphology can be well-dispersed in ethanol to form colloidal solutions. The CeF_3, CeF_3:Tb^{3+}, and CeF_3:Tb^{3+}/LaF_3 (core/shell) nanoparticles show characteristic emission of Ce^{3+} (5d−4f) and Tb^{3+} (f−f), respectively. The luminescent intensity and lifetime of the CeF_3:Tb^{3+}/LaF_3 core/shell nanoparticles is greatly enhanced with respect to the bare CeF_3:Tb^{3+} nanoparticles because the nonradiative processes at or near the surface of the nanoparticles are much reduced. The strong green emission of Tb^{3+} in CeF_3:Tb^{3+} and CeF_3:Tb^{3+}/LaF_3 nanoparticles results from an efficient energy transfer from Ce^{3+} to Tb^{3+}, in which the critical distance is about 0.46 nm. These nanoparticles can be potentially used as labels for biological molecules.

Acknowledgment. This project is financially supported by the foundation of "Bairen Jihua" of Chinese Academy of Sciences, the MOST of China (2003CB314707), and the National Natural Science Foundation of China (NSFC 50225205, 50572103, 20431030). J.F. is grateful for the financial support by the foundation of a two-base program for international cooperation of NSFC (00310530) related to Project 50225205, and NSF DMR-0449580.

CM052360X

(22) Wang, Z. L.; Quan, Z. W.; Lin, J.; Fang, J. *J. Nanosci. Nanotech.* **2005**, *5*, 1532−1536.

(23) (a) Thomas, K. S.; Singh, S.; Dieke, G. H. *J. Chem. Phys.* **1963**, *38*, 2180−2190. (b) Blasse, G. *Mater. Chem. Phys.* **1987**, *16*, 201−236. (c) Blasse, G. *Philips Res. Repts.* **1969**, *24*, 131−144. (d) Jia, P. Y.; Yu, M.; Lin, J. *J. Solid State Chem.* **2005**, *178*, 2734−2740.